A short note on the discontinuous Galerkin discretization of the pressure projection operator in incompressible flow

D.T. Steinmoeller[a,*], M. Stastna[a], K.G. Lamb[a]

[a] *200 University Ave. W., Waterloo, ON, N2L 3G1*

Abstract

This note reports on the issue of spurious compressibility artifacts that can arise when the popular pressure projection (PP) method is used for unsteady simulations of incompressible flow using the symmetric interior penalty discontinuous Galerkin (SIP-DG) method. Through a spectral analysis of the projection operator's SIP-DG discretization, we demonstrate that the eigenfunctions of the operator do not form a basis that allows for the correct enforcement of the incompressibility constraint. This short-coming can cause numerical instabilities for inviscid, advection-dominated, and density stratified flow simulations, especially for long-time integrations and/or under-resolved situations. To remedy this problem, we propose a local post-processing projection that enforces incompressibility exactly, thereby enhancing the stability properties of the method.

Keywords: Incompressible Navier–Stokes Equations, Projection Methods, Discontinuous Galerkin Method, High-order element methods, Boussinesq Approximation, Non-hydrostatic Flow

1. Introduction

Recent interest in the possibility of using the discontinuous Galerkin (DG) method for numerical solutions to the unsteady incompressible Navier–Stokes (INS) equations has been sparked by its success in compressible

*Corresponding author at: Department of Applied Mathematics, University of Waterloo, Waterloo, ON, Canada. N2L 3G1. Tel.: +1 519 888 4567 ext. 32588; fax: +1 519 746 4319.

Email address: dsteinmo@uwaterloo.ca (D.T. Steinmoeller)

Preprint submitted to Journal of Computational Physics *April 23, 2013*

flow simulations [1, 2, 3] and its many attractive features such as geometric flexibility, stencil locality/compactness, upwind-biased fluxes for advection-dominated flows, and high-order accuracy [3, 4, 5]. The desire for DG solutions is further motivated by the Ladyzhenskaya-Babuska-Brezzi (LBB) stability problem that plagues continuous Galerkin (CG) formulations due to spurious pressure modes, resulting in stability for only certain spatially mixed-order velocity-pressure formulations [6, 7, 8, 9].

However, since the INS equations do not comprise a hyperbolic system it is unclear if the DG method can be used to recover consistent, stable, and accurate numerical solutions in general, since DG methods only weakly impose continuity across elemental interfaces, typically by solving Riemann problems to specify an appropriate numerical flux function [3]. Indeed, for the spectral element ocean model (SEOM), Levin *et al.* [10] chose a DG formulation for scalar transport equations but not for the momentum equations, citing the ill-posedness of the Riemann problem as a central difficulty. On the other hand, some studies have successfully obtained DG solutions, using the pressure projection (PP) method, to some standard test cases for the INS equations, such as the Taylor-Green Vortex [3, 11, 12], laminar Kovasznay flow [3], and flow past square [11, 12] and circular [3] cylinders. These test cases, however, typically focus on short time integrations or highly viscous/damped situations, and the long-term stability properties of the methods remain unclear.

More work needs to be done to explore weakly damped and inviscid cases with DG, since some promise has already been shown using the closely-related spectral multi-domain penalty method (SMPM) in the vertical coordinate for simulations of stratified turbulence in incompressible flow [13]. The SMPM differs from the DG method only in the sense that a collocation formulation is used instead of a Galerkin formulation, but the other basic concepts of the schemes (e.g., locally high-order polynomial methods, continuity between subdomains only weakly enforced) are the same [14].

Here, we focus on difficulties encountered when using the standard PP for the INS equations in velocity-pressure formulation for longer time integrations of non-hydrostatic stratified flow simulations under the Boussinesq approximation (BA). These difficulties are especially prevalent in under- to marginally-resolved inviscid or low-viscosity situations. The main contribution of this work is a spectral analysis of the DG PP operator that is furnished by the numerical calculation of the eigenvalues and eigenfunctions on a unit square domain with solid-wall boundary conditions. We also demonstrate that a local post-processing projection can be used to exactly enforce incompressibility, thereby stabilizing the method for longer time integrations. We argue that the results shown here are robust and apply to more general domains and meshes as well as to the three-dimensional INS equations.

2. Methods

2.1. Pressure Projection (PP) Method and its weak form

The non-dimensional stratified INS equations under the BA are [15]

$$\begin{aligned} \frac{\partial \mathbf{u}}{\partial t} + \nabla \cdot (\mathbf{u} \otimes \mathbf{u}) &= -\nabla p + \frac{1}{Re}\nabla^2 \mathbf{u} - \frac{1}{Fr^2}\rho \mathbf{k} \,, & (1) \\ \nabla \cdot \mathbf{u} &= 0 \,, & (2) \\ \frac{\partial \rho}{\partial t} + \nabla \cdot (\rho \mathbf{u}) &= 0 \,, & (3) \end{aligned}$$

corresponding to conservation of momentum (1) and mass (2), and scalar transport (3). Here, $\mathbf{u}$ is the dimensionless velocity field with components $(u(\mathbf{x}, t), w(\mathbf{x}, t))$ (and $\mathbf{x} = (x, z)$) in two dimensions, $\mathbf{k}$ is the unit vector pointing along the positive z-axis, and $p = p(\mathbf{x}, t)$ and $\rho = \rho(\mathbf{x}, t)$ are the dimensionless pressure and density, respectively. $Re = UL/\nu$ is the Reynolds number as a function of kinematic viscosity ν and typical velocity and length scales U and L, respectively. The Froude number is defined by $Fr = U/\sqrt{gL}$, where g is the gravitational acceleration, and we have chosen the advective time-scale $T = L/U$ in our non-dimensionalization. The inviscid incompressible Euler (IE) equations are recovered in the limit $Re \to \infty$, and the case of non-buoyancy-driven flow is recovered by taking $Fr \to \infty$. The essence of the Boussinesq approximation (BA) is that in the momentum equations, the density is taken as a constant in all but the buoyancy term.

The PP time-stepping algorithm has been thoroughly explained in the literature (see e.g., [16]). A very popular approach is the high-order stiffly-stable splitting algorithm due to Karniadakis *et al.* [17]. The method first forms a predicted velocity $\hat{\mathbf{u}}$ by explicitly evolving the advection and buoyancy terms with a linear multi-step method. The projection step involves solving the following Poisson equation, along with suitable boundary conditions (see [17]), for the pressure p at time $t_{n+1} = t_n + \Delta t$:

$$\nabla \cdot \hat{\hat{\mathbf{u}}} - \nabla \cdot \hat{\mathbf{u}} = -\Delta t \nabla^2 p^{n+1} \,. \quad (4)$$

Here $\hat{\hat{\mathbf{u}}}$, is an intermediate velocity that is formed after the pressure terms have been evolved, but before the viscous step. The constraint (2) is enforced by removing the $\nabla \cdot \hat{\hat{\mathbf{u}}}$ term in (4), thereby projecting the approximate solution onto the space of approximately non-divergent velocity fields. Once p^{n+1} has been computed, the pressure gradient is evolved in the semi-discrete form of (1) to recover the corrected velocity field,

$$\hat{\hat{\mathbf{u}}} = \hat{\mathbf{u}} - \Delta t \nabla p^{n+1} , \tag{5}$$

and the viscous terms can subsequently be evolved to recover $\mathbf{u}^{n+1}$, often using implicit time-stepping from the backward differentiation formula (BDF) family of time integrators[1].

In the context of DG methods, the difficulty highlighted in this work stems from the discretization of the left-hand side of (4), and we presuppose that the right-hand side is discretized via the nodal symmetric interior penalty DG (SIP-DG) method (see [3] for an overview and a MATLAB implementation). The weak DG formulation of the left-hand side can be found by considering the local solution to (4) on a particular element (or sub-domain of Ω) D^k (where $k = 1, \cdots, K$), multiplying by a member of the space of local test-functions $\{\phi_j^k\}_{j=1}^{N_p}$ and integrating by parts to yield

$$\left(\int\limits_{\partial D^k} \left(\phi_j^k \hat{\hat{\mathbf{u}}}\right)^* \cdot \hat{\mathbf{n}}\, d\mathbf{x} - \int\limits_{D^k} \hat{\hat{\mathbf{u}}}^k \cdot \nabla \phi_j^k \, d\mathbf{x} \right) - \left(\int\limits_{\partial D^k} (\phi_j \hat{\mathbf{u}})^* \cdot \hat{\mathbf{n}}\, d\mathbf{x} - \int\limits_{D^k} \hat{\mathbf{u}}^k \cdot \nabla \phi_j^k \, d\mathbf{x} \right) , \tag{6}$$

where superscript $*$ denotes an appropriate numerical flux function chosen to impose weak continuity across element interfaces in a way that is consistent with the underlying dynamics of the INS equations.

We notice that the PP method results in simply removing the first two terms in eqn. (6). Thus, the divergence-free constraint is only being imposed upon the corrected velocity $\hat{\hat{\mathbf{u}}}$ in a weak and local sense, and the overall impact on the resulting DG scheme remains unclear. Here, we attempt to understand the effects of using the PP with DG via a numerical eigenvalue analysis as explained below.

[1] In the DG framework, this last step is usually discretized using the SIP-DG formulation of the implicit viscosity operator $\left[1 - (\beta_0 \Delta t / Re)\nabla^2\right]$ subject to the no-slip boundary condition $\mathbf{u} = 0$ on solid boundaries [3, 11, 12], where β_0 depends on which BDF method is used.

2.2. Numerical Method for the Eigenvalue Analysis

Beginning with the nodal DG implementation of the INS solver presented in [3], we have computed the eigenvalues of the PP operator $\mathbb{P} : \hat{\mathbf{u}} \mapsto \mathbf{u}^{n+1}$ that carries out the following linear operations in a single MATLAB function:

1. Given the input $\hat{\mathbf{u}}$, solve for p^{n+1} using the SIP-DG discretization of the Poisson problem (4) with the $\nabla \cdot \hat{\hat{\mathbf{u}}}$ term dropped.
2. Calculate the discretized form of ∇p^{n+1}, and use eqn. (5) to obtain $\hat{\hat{\mathbf{u}}}$.
3. If Re is finite, advance the viscous term using SIP-DG discretization of the viscosity operator to recover the output, $\mathbf{u}^{n+1}$.
   If Re is infinite, set $\mathbf{u}^{n+1} = \hat{\hat{\mathbf{u}}}$.

The corresponding function-handle is then passed into MATLAB's `eig` eigenvalue solver that calculates eigenvalues using the implicitly-restarted Arnoldi method implemented in the `ARPACK` Fortran77 library [18]. It is worth noting that since the pressure variable p is not a prognostic flow variable and its purpose is to simply enforce incompressibility on $\mathbf{u}$ (see [16]), it is treated as an auxiliary field by the $\mathbb{P}$ operator.

The domain under consideration is the closed unit square $\Omega = [0, 1]^2$ subject to no normal flow (no slip) boundary conditions for the inviscid (viscous) case. For a domain with solid walls only, the Poisson problem (4) is subject to Neumann conditions only, and there is no unique solution [17]. To address this issue, we have adopted the approach of [19], where a small additive scalar unknown is added to (4) in order to impose the additional constraint of zero mean pressure. Alternatives to this approach, including null singular vector removal, are possible as well. See [14] for an overview in the context of the SMPM method.

Eqn. (4) itself is solved by computing the LU-factorization of the discrete Laplacian during pre-processing for re-use during each `eig` iteration. Throughout this note, we have chosen to solve the linear systems directly. We leave the issue of using an iterative linear solver, and the associated complexities (e.g., pre-conditioning), to a future work.

3. Results

3.1. DG Simulations using the PP method

We have carried out long-time integrations of the homogeneous ($\rho = constant$, $Fr \to \infty$) form of (1)-(2) using the nodal DG implementation in [3] and found spikes in the solution that form at element interfaces and eventually lead to numerical instability. Modal filtering [3] alleviates the issue somewhat, but does not prevent instabilities in general. Plotting the divergence $\nabla \cdot \mathbf{u}$ suggests the issue is related to spurious compressibility artifacts near element interfaces that are not zero to numerical precision. This behaviour is a consequence of the fact that incompressibility is only imposed in a local weak sense, and hence the numerical solution is inconsistent with the INS equations since $\nabla \cdot \mathbf{u} \neq 0$ to working precision.

For stratified flow simulations under the BA, the situation is worse since the presence of an active density tracer, ρ, in the vertical momentum equation implies that any numerically-driven perturbation to ρ will cause spurious vertical motion. In under-resolved cases, we found that spurious compressions caused regions of high density to artificially emerge over regions of low density at certain element interfaces, resulting in unphysical grid-scale Rayleigh-Taylor (RT) instabilities [15] that destroyed the numerical solution. In marginally- to well-resolved simulations, the unphysical RT instabilities appear to be suppressed. However, the long-term stability properties are again uncertain due to non-zero divergence.

3.2. Spectral analysis of the DG PP operator and proposed remedies to the problem

The unit square domain Ω was partitioned into 8 uniform triangular elements, and the eigenvalues and eigenfunctions (velocities), $(\lambda_i, \mathbf{u}_{\phi_i})_{i=1}^{N_e}$ of the PP operator $\mathbb{P}$ were computed for polynomial order $N = 8$ corresponding to $N_p = 45$ nodal points on each triangle [3], for a total of 360 grid points yielding $N_e = 720$ eigenmodes. The eigenspectrum was computed for a variety of Re as well as for the inviscid case. Each velocity field was scaled such that $\int_\Omega \|\mathbf{u}_{\phi_i}\|^2 \, d\mathbf{x} = 1$. Although this analysis has been carried out for triangular elements, the procedure extends straightforwardly to other types of elements, e.g., quadrilaterals.

To assess the properties of the eigenmodes, in Fig. 1 we plot the quantity

$$D_i = \left(\int_\Omega \left[\nabla \cdot \mathbf{u}_{\phi_i}\right]^2 \, d\mathbf{x} \right)^{\frac{1}{2}} \left[\max_{1 \le j \le N_e} \left(\int_\Omega \left[\nabla \cdot \mathbf{u}_{\phi_j}\right]^2 \, d\mathbf{x} \right)^{\frac{1}{2}} \right]^{-1}, \tag{7}$$

the scaled L^2-norm of divergence in each velocity eigenfunction $\mathbf{u}_{\phi_i}$ against its corresponding eigenvalue, λ_i. The integrals in eqn. (7) were evaluated using the orthogonality of the basis functions in the local modal expansion.

Perhaps the most revealing result in Fig. 1 is the inviscid case shown in panel **(c)**. Since the inviscid $\mathbb{P}$ operator includes only the projection and not viscosity, we find that there are only two possible eigenvalues, $\lambda = 1$ and $\lambda = 0$, each with its own collection of corresponding eigenfunctions. To understand the structure of the degeneracy of the eigenspectrum of the inviscid projection operator, it is useful to recall the Helmholtz decomposition that guarantees any vector field may be decomposed into the sum of curl-free and divergence-free components

$$\mathbf{u} = -\nabla\varphi + \nabla \times (\psi\mathbf{j}) \ , \tag{8}$$

where the unit vector $\mathbf{j} = (0, 1, 0)$ appears since we assume $\mathbf{u}$ lies in the xz-plane. The $\mathbb{P}$ operator should map vector fields of the general form (8) to the divergence-free part $\nabla \times (\psi\mathbf{j})$. Two special cases that arise from this fact are: (1) If $\mathbf{u}_{\phi_i}$ is an eigenfunction of $\mathbb{P}$ with no curl-free part, then $\mathbb{P}$ should not change it, hence $\lambda = 1$, and (2) if $\mathbf{u}_{\phi_i}$ is an eigenfunction of $\mathbb{P}$ with no divergence-free part, then $\mathbb{P}$ should map it to $\mathbf{0}$, i.e., it belongs in the null space ($\lambda = 0$) of $\mathbb{P}$. Therefore, the inviscid $\lambda = 0$ eigenmodes should be interpreted as a basis of curl-free velocities while the inviscid $\lambda = 1$ eigenmodes should be interpreted as a basis of divergence-free velocities.

The key thing to notice here is that the discretized eigenfunctions forming a basis for incompressible velocity fields are themselves not divergence-free since they have $D_i \neq 0$. In Fig. 2, we show contour plots of the scaled absolute value of the divergence of two such eigenfunctions to illustrate this undesired behaviour that is worst at element interfaces. In light of these results, it is not clear if we can represent an incompressible velocity field using such a basis and expect it to be genuinely divergence-free. The finite Re cases in Fig. 1 show that viscosity introduces eigenmodes with $0 < \lambda < 1$. These eigenvalues between 0 and 1 should be expected since in the simplified case of periodic boundary conditions, the viscosity operator would effectively multiply the sinusoid e^{ikx} by $[1 - (\beta_0\Delta t/Re)k^2]$. Although viscosity does not yield eigenmodes with smaller values of D_i, sufficiently small Re will ensure that the eigenspectrum is structured such that smaller eigenvalues ($\lambda_i < 1$) are assigned to eigenfunctions with larger values of D_i. This can be seen as beneficial since the most poorly behaved eigenmodes are marginalized in the eigendecomposition of $\mathbb{P}$. Of particular note is the absence of $O(1)$ values of D_i for $\lambda_i \approx 1$ in the $Re = 1$ and $Re = 40$ cases. Despite these results, it remains unclear how much viscosity is required to attain long term stability in general because viscosity does not correct the problem of spurious divergence. Instead, it provides a rather general mechanism for damping small-scale numerical artifacts.

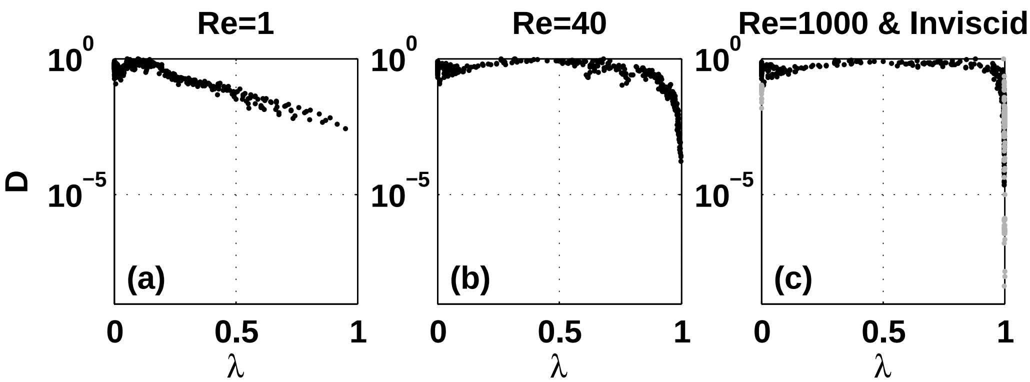

Figure 1: D_i, eigenfunction's scaled maximum L^2-norm of divergence vs. corresponding eigenvalue λ_i at selected Re and in the inviscid case, $Re \to \infty$ (panel **(c)**, grey dots). For finite Re, we set $\beta_0 \Delta t = 10^{-3}$.

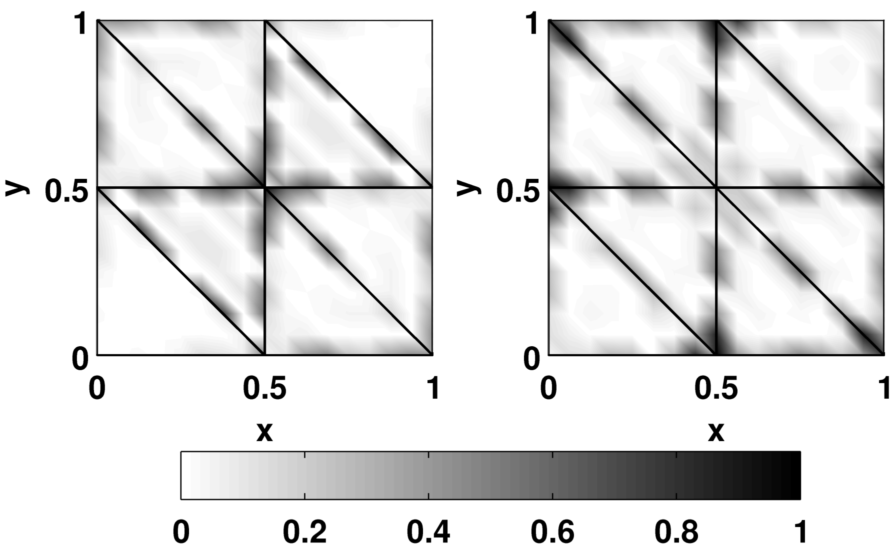

Figure 2: Absolute value of divergence $|\nabla \cdot \mathbf{u}_{\phi_i}|$ (re-scaled to have maximum value of 1) for two selected eigenfunctions of the inviscid $\mathbb{P}$ operator (see Fig. 1 **(c)**) with corresponding eigenvalue $\lambda_i = 1$ (to within 5 decimal places).

Approaches adopted in the literature to circumvent the problem highlighted above avoid the PP altogether, and ensure that the weak form of the divergence-free constraint explicitly appears in the scheme along with a suitable numerical flux function ([20, 21, 22]). Cockburn *et al.* [22] use a pressure stabilization term in their numerical flux choice for the weak DG form of (2) along with a post-processing procedure to obtain exactly non-divergent approximate velocity fields to solve the steady INS equations. The method of [20, 21] recovers a well-posed Riemann problem in the imposition of (2) by considering a numerical flux function from the artificial compressibility equations[2]. However, the method appears somewhat costly since all terms are discretized implicitly in time and exact Riemann problems must be solved numerically by nonlinear Newton iterations at each time-step. Other possibilities lie with the recently discussed class of hybridizable DG (HDG) methods [23, 24], that impose strong continuity only in the normal component of numerical fluxes. Finally, for strictly two-dimensional flow, a streamfunction-vorticity formulation could be adopted. This idea has been explored in a DG context in [25].

In the present work, we have followed up on the theoretical developments in [22] wherein it is proven that stable equal-order DG schemes for the steady INS equations require (i) a pressure stabilization term in the DG discretization of (2), and (ii) a local post-processing operation to recover an exactly non-divergent velocity field from the weakly non-divergent velocity field. Here, we attempt to apply these results in the unsteady case. In the SIP-DG framework discussed above, condition (i) is already satisfied since the SIP-DG discretization of the Laplacian uses a stabilization (or penalty) term in the numerical flux function of an auxiliary vector variable $\mathbf{q} = \nabla p$ to penalize large jumps in p. Here, the SIP-DG numerical flux functions are given by $p^* = \{\{p\}\}$ and $\mathbf{q}^* = \{\{\nabla p\}\} - \tau[\![p]\!]$, where $\tau > 0$ is the penalty parameter [3], and the operators $\{\{\cdot\}\}$ and $[\![\cdot]\!]$ denote the average and jump across an interface, respectively. Therefore, it appears that a missing ingredient in the scheme discussed above is the local post-processing projection, and we have sought to rectify this issue.

A locally non-divergent velocity basis on the reference element can be constructed by an appropriate differentiation of the modal basis functions ψ_i that, as in [3], are orthogonal polynomials of order N. In two-dimensions,

[2]The artificial compressibility equations can be recovered by adding a $\epsilon^2 \frac{\partial p}{\partial t}$ term to the left-hand side of 2, where $\epsilon = U/c$ is a Mach number and c is an artificial sound speed.

the velocity basis is taken to be

$$\mathbf{u}_{\psi_i} = \nabla \times (\psi_i \mathbf{j}) \ , \quad i = 1, \cdots, N_m \ , \tag{9}$$

where N_m is the number of local modal basis functions (we omit the $\psi_i =$ *constant* mode), and $\mathbf{j} = (0, 1, 0)$. The unit vector $\mathbf{j}$ appears here since the resulting velocity basis should lie in the xz-plane, i.e., the same plane as the velocity field. By construction, we have $\nabla \cdot \mathbf{u}_{\psi_i} = 0$ for $i = 1, \cdots, N_m$, and we have verified that the local discrete differential operators satisfy this condition to numerical precision. Although the basis (9) is a set of vectors and not scalars as is common with DG and CG methods, a Galerkin-type projection can be furnished on the reference element by considering an arbitrary divergence-free velocity field $\mathbf{v}$ expanded in terms of the basis (9):

$$\mathbf{v} = \sum_{j=1}^{N_m} c_j \mathbf{u}_{\psi_j} \ , \quad j = 1, \cdots, N_m \ . \tag{10}$$

The c_j's can be computed by taking the dot product of (10) with a member of the divergence-free velocity basis $\mathbf{u}_{\psi_i}$, integrating over the reference element Γ, and inverting the resulting linear system of equations

$$M_{ij} c_j = l_i \ , \tag{11}$$

where

$$M_{ij} = \int_{\Gamma} \mathbf{u}_{\psi_i} \cdot \mathbf{u}_{\psi_j} \, d\mathbf{x} \ , \quad l_i = \int_{\Gamma} \mathbf{u}_{\psi_i} \cdot \mathbf{v} \, d\mathbf{x} \ . \tag{12}$$

Therefore, any arbitrary velocity $\mathbf{u}$ defined on the reference element can be projected onto the space of exactly non-divergent velocities by solving (11), with $\mathbf{v}$ replaced by $\mathbf{u}$ in (12), and summing the right-hand side of (10) to recover $\mathbf{v}$, an exactly divergence-free approximation to the non-divergent part of $\mathbf{u}$. As in [22], the operation of mapping $\mathbf{u}$ to $\mathbf{v}$ is completely local and can be carried out in an element-by-element fashion once the local velocity on each element has been transformed to the standard element's coordinate system. Should this projection be extended to three dimensions, it is worth noting that special care should be taken to ensure that the solenoidal basis spans all of three-space. The corresponding basis would need to be made as much as three times larger than the basis (9), since those vectors are restricted to a single plane.

In Fig. 3, we show the strong impact that applying the post-processing projection has on the eigenspectrum of the $\mathbb{P}$ operator. All eigenmodes except those corresponding to the null space of $\mathbb{P}$ satisfy $\nabla \cdot \mathbf{u}_\phi = 0$ to numerical precision.

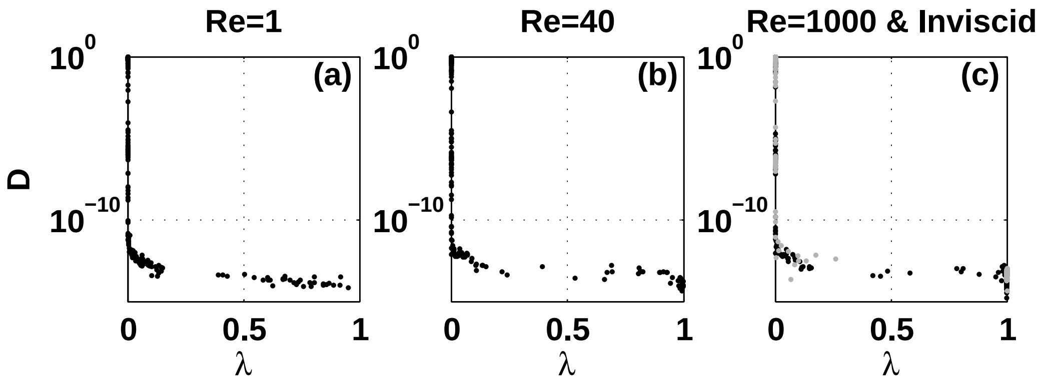

Figure 3: Like Fig. 1, but the post-processing operator has been applied at the end of the usual $\mathbb{P}$ operation.

3.3. Validation in two space dimensions

We have modified the INS solver presented in [3] to solve the incompressible Euler (IE) equations under the Boussinesq Approximation (BA). The advection and source terms are evolved with the third order Adams-Bashforth method. The Lax-Friedrichs/Rusanov advective flux is employed in the DG discretization of the advective terms, as in [3]. An exponential cut-off filter function (see [3]) is applied to the local modal coefficients of the full solution fields after the advective step to prevent polynomial aliasing errors from driving weak instabilities.

We have successfully validated the method for the stratified IE BA equations against the Fourier spectral method benchmark laboratory-scale internal solitary wave (ISW) solutions to the Dubreil-Jacotin-Long (DJL) equation found in [26]. Although the solution profile simply translates to the right with constant speed $c = 0.1042$ ms^{-1}, the dynamics are driven by nonlinear and non-hydrostatic effects. The geometry is a given by a simple rectangle with dimensions 5 m $\times 0.15$ m taken to be periodic in x and bounded by rigid horizontal walls at $z = 0$ and $z = -0.15$ m; nevertheless, this test-case is challenging since the horizontal:vertical aspect ratio is $\sim$33:1, and high amounts of vertical resolution are required to properly resolve the thin pycnocline.

We have constructed a structured grid of $1,089$ rectangular elements and carried out DG simulations using polynomial orders $N = 4$ (marginally resolved) and $N = 8$ (well-resolved), both with the local projection (WLP) discussed in Sec. 3.2 and without (NLP). Here, we have used rectangular elements since we were able to reach the requisite resolution with a smaller number of elements than would be necessary with a structured or unstructured triangular mesh. For the cases considered here, the added computational time associated with including the local projection was negligible. The local modal filtering parameters were taken to be $(s, N_c) = (4, 4)$ in the $N = 4$ case and $(s, N_c) = (8, 6)$ for $N = 8$. Here, s is the order of the exponential filter function and N_c is the cut-off order, below which no filtering takes place. In particular, these parameters imply that for the $N = 4$ simulations, 9 of 25 modes are unaffected by the filter, while 30 of 81 modes are unaffected in the $N = 8$ case. The initial solution fields (ρ, u, w) were interpolated from the equispaced Fourier grid to our DG grids via a band-limited spectral interpolation code[3].

The results shown in Fig. 4**(a)**-**(b)** demonstrate that the method accurately captures the propagation of the ISW. The long-term stability properties of the methods are assessed in panel **(c)** where we plot the L^2-norm of the divergence vs. time in each case. The $N = 4$ NLP case becomes unstable by $t = 160$ s, and the $N = 4$ WLP case becomes unstable by $t = 240$ s (not pictured). This result indicates that local projection has improved the stability properties of the $N = 4$ scheme somewhat, but it is not sufficient for long-term stability in this case due to element-scale noise introduced as a result of under-resolution. Both the WLP and NLP $N = 8$ cases appear long-term stable, since the L^2-norm of divergence in the NLP case demonstrates a damped limit-cycle type behaviour for times longer than those reported in Fig. 4 (not shown). The two stable runs from Fig. 4 were integrated out to a final time of $t = 600$ s, when the wave has travelled a distance of 62.52 m (or ≈ 12.5 domain lengths). A more complete set of test cases (including viscous simulations) with more thorough analysis of results and details on the numerical solver will become available in a forthcoming publication.

[3]The code `bandLimFourierInterp` is freely available at: `https://github.com/dsteinmo/bandLimFourierInterp/`.

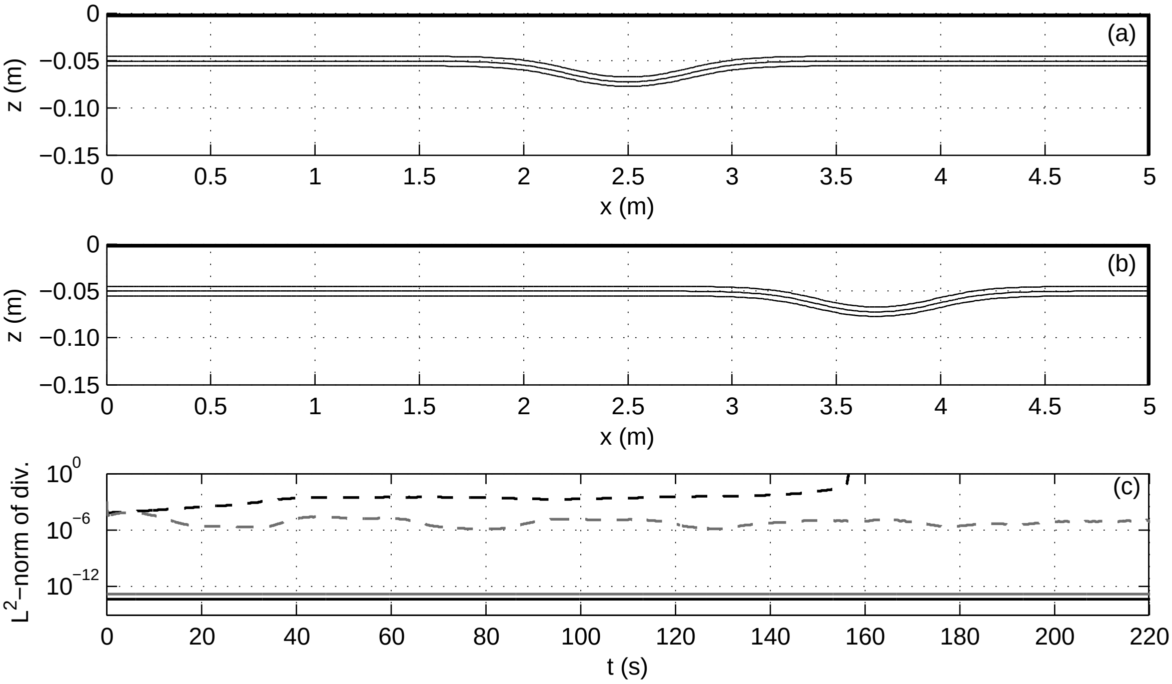

Figure 4: The position of the thin pycnocline is indicated by three contour lines of non-dimensional density ρ for the DJL ISW test case at times **(a)** $t = 0$ s and **(b)** $t = 540$ s using the $N = 8$ WLP method. Panel **(c)** shows the L^2-norm of divergence vs. time for the methods: $N = 4$ WLP (black, solid), $N = 4$ NLP (black, dashed), $N = 8$ WLP (grey, solid), and $N = 8$ NLP (grey, dashed).

4. Conclusions

Through a numerical eigenvalue analysis, we have shown that the eigenfunctions of the DG PP operator are themselves not divergence-free. As a result, our numerical simulations have shown that instabilities can occur due to the presence of spurious compressibility artifacts. The prominence of these instabilities appears to be worse in poorly resolved simulations. It was found that even if incompressibility is enforced exactly after each time-step by a local post-processing projection, that polynomial orders $N > 4$ were required for long-term stability in the test-case considered here. It may be possible to further remedy the stability issues highlighted here. Remedies discussed in other works include considering the artificial compressibility equations to formulate a suitable numerical flux function [20, 21], or pursuing an HDG spatial discretization method [23, 24].

Acknowledgement

The research is supported by the Natural Sciences and Engineering Research Council of Canada through Discovery Grants to MS and KGL. DTS was supported by an Ontario Graduate Scholarship. Constructive suggestions from Peter J. Diamessis (Cornell University) are gratefully acknowledged.

References

[1] F. Bassi, S. Rebay, A high-order accurate discontinuous finite element method for the numerical solution of the compressible Navier-Stokes equations, J. Comp. Phys. 131 (1997) 267–279.

[2] F. X. Giraldo, M. Restelli, A study of spectral element and discontinuous Galerkin methods for the Navier-Stokes equations in nonhydrostatic mesoscale atmospheric modeling: Equation sets and test cases, J. Comp. Phys. 227 (2008) 3849–3877.

[3] J. Hesthaven, T. Warburton, Nodal Discontinuous Galerkin Methods, Springer, 2008.

[4] B. Cockburn, S. Hou, C. Shu, The Runge–Kutta local projection discontinuous Galerkin finite-element method for conservation-laws. 4. the multidimensional case, Math. Comp 54 (1990) 545–581.

[5] B. Cockburn, C. Shu, TVB Runge–Kutta local projection discontinuous Galerkin finite-element method for conservation-laws. 2. General framework, Math. Comp. 52 (1989) 411–435.

[6] C. J. Cotter, D. A. Ham, C. C. Pain, S. Reich, LBB stability of a mixed Galerkin finite element pair for fluid flow simulations, J. Comp. Phys. 228 (2009) 336–348.

[7] E. Hanert, R. Walters, D. Le Roux, J. Pietrzak, A tale of two elements: P1ncP1 and RT0, Ocean Modelling 28 (2009) 24–33.

[8] M. Iskandarani, D. Haidvogel, J. Boyd, A staggered spectral element model with application to the oceanic shallow-water equations, Int. J. Numer. Meth. Fluids 20 (1995) 393–414.
[9] M. Iskandarani, D. Haidvogel, J. Levin, A three-dimensional spectral element model for the solution of the hydrostatic primitive equations, J. Comp. Phys. 186 (2003) 397–425.
[10] J. C. Levin, M. Iskandarani, D. B. Haidvogel, To continue or discontinue: Comparisons of continuous and discontinuous Galerkin formulations in a spectral element ocean model, Ocean Modelling 15 (2006) 56–70.
[11] E. Ferrer, R. Willden, A high order Discontinuous Galerkin Finite Element solver for the incompressible Navier–Stokes equations, Comput. Fluids 46 (2011) 224–230.
[12] K. Shahbazi, P. Fischer, C. Ethier, A high-order discontinuous Galerkin method for the unsteady incompressible Navier–Stokes equations, J. Comp. Phys 222 (2007) 391–407.
[13] P. Diamessis, J. Domaradzki, J. Hesthaven, A spectral multidomain penalty method model for the simulation of high Reynolds number localized incompressible stratified turbulence, J. Comp. Phys. 202 (2005) 298–322.
[14] J. Escobar-Vargas, A spectral multidomain penalty method solver for environmental flow processes, Ph.D. thesis, Cornell University, Ithica, NY, USA, 2012.
[15] P. Kundu, I. Cohen, Fluid Mechanics, Elsevier Academic Press, 4 edition, 2008.
[16] A. Almgren, J. Bell, W. Crutchfield, Approximate projection methods: Part I. inviscid analysis, SIAM J. Sci. Comput. 22 (2000) 1139–1159.
[17] G. Karniadakis, M. Israeli, S. Orszag, High-order splitting methods for the incompressible Navier–Stokes equations, J. Comp. Phys. 97 (1991) 414–443.
[18] R. B. Lehoucq, D. C. Sorensen, C. Yang, ARPACK users' guide: Solution of large scale eigenvalue problems with implicitly restarted Arnoldi methods, 1997.
[19] U. Trottenberg, C. Oosterlee, A. Schuller, Multigrid, Academic Press, 1st edition, 2000.
[20] F. Bassi, A. Crivellini, D. A. Di Pietro, S. Rebay, An artificial compressibility flux for the discontinuous Galerkin solution of the incompressible Navier–Stokes equations, J. Comp. Phys 218 (2006) 794–815.
[21] F. Bassi, A. Crivellini, D. A. Di Pietro, S. Rebay, An implicit high-order discontinuous Galerkin method for steady and unsteady incompressible flows, Comput. Fluids 36 (2007) 1529–1546.
[22] B. Cockburn, G. Kanschat, D. Schötzau, An equal-order DG method for the incompressible Navier–Stokes equations, J. Sci. Comput. 40 (2009) 188–210.
[23] N. Nguyen, J. Peraire, Hybridizable discontinuous Galerkin method for partial differential equations in continuum mechanics, J. Comp. Phys. 231 (2012) 5955–5988.
[24] S. Rhebergen, B. Cockburn, A space–time hybridizable discontinuous Galerkin method for incompressible flows on deforming domains, J. Comp. Phys. 231 (2012) 4185–4204.
[25] J.-G. Liu, C.-W. Shu, A high-order discontinuous Galerkin method for 2D incompressible flows, J. Comp. Phys. 160 (2000) 577–596.
[26] M. Dunphy, C. Subich, M. Stastna, Spectral methods for internal waves: indistinguishable density profiles and double-humped solitary waves, Nonlin. Proc. Geoph.

18 (2011) 351–358.